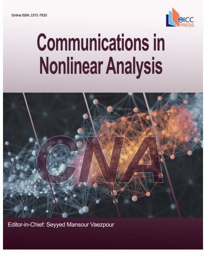

Commun. Nonlinear Anal. 2025; 13(2) : 75-86

Communications in Nonlinear Analysis

https://doi.org/cna.2025.hpsm-8n90

Research Article

A Novel Approach in Elastic Flight Simulation of a Slender Flexible Vehicle to Assess the Role of Thrust Deviations in Stability

Hossein Faveadi[1], Alireza Davari[1,*], Farshad Pazooki[1], Majid Pouladian[2]

[1]*Department of Mechanical and Aerospace Engineering, SR.C, Islamic Azad University, Tehran, Iran*
[2]*Department of Medical Engineering, SR.C, Islamic Azad University, Tehran, Iran*

[*]**Corresponding author:** ardavari@srbiau.ac.ir

Article History

Received:
2024-08-11

Revised:
2024-10-30

Accepted:
2025-01-16

Published online:
2025-06-30

© 2025 The Author(s). Published by the OICC Press under the terms of the CC BY 4.0, Creative Commons Attribution License, which permits use, distribution and reproduction in any medium, provided the original work is properly cited.

Abstract:

Purpose: Because of the linearized and simplified models, many of the existing methods for stability analysis cannot accurately simulate the real flight behavior of the flexible vehicles, so non-linear models with minimum simplification should be employed instead. However, due to the need to simultaneously solve coupled complex structural and aerodynamic equations in each time step, such models require massive calculations, greatly reducing the simulation speed and increasing the run time.

Approach: In this research, the volume of computations in each time step was reduced by appropriate lookup tables made from some pre-performed calculations, and as a result, a higher execution speed of the simulation was achieved. With this new strategy, the role of various design inputs, such as structure stiffness, which is usually represented by the natural frequency, exerted maneuvering acceleration, propulsion force function, and roll speed on trajectory, collision accuracy, and flight stability of a flexible projectile can be achieved. Only the role of thrust function and structure flexibility has been addressed in this research.

Findings: The results show that the inherent inaccuracies in the thrust force (inherent deviation and out-centering) and reduction of the natural frequencies increase the effect of aeroelasticity and the probability of the flight instability of the projectile in open-loop flights.

Originality/Value: General (Classic) flight simulations often neglect elastic properties, which can sometimes result in significant errors. Taking the aeroelasticity into account would result in massive calculations and computational time costs, on the other hand. This paper makes the simulation velocity much faster (to somehow close to a rigid projectile simulation) by using some pre-prepared look-up tables from existing aeroelastic run-time computations. This method has not been employed in similar aeroelastic calculations reported in the literature.

Keywords: Flight simulation; Aeroelasticity; Lookup tables; Flexible projectile; Time domain stability analysis. MSC 2020: 74F10; 70Q05

Cite this article: Faveadi H., Davari A., Pazooki F., Pouladian M. A Novel Approach in Elastic Flight Simulation of a Slender Flexible Vehicle to Assess the Role of Thrust Deviations in Stability. Communications in Nonlinear Analysis 2025; *13*(2): 75-86 https://doi.org/PLACEHOLDER

1. Introduction

Aeroelasticity is expressed as the interaction between aerodynamic and structural deformations and is divided into static and dynamic. In static aeroelasticity, the inertial loads (structural vibrations) are ignored. In contrast, in dynamic aeroelasticity, the deformation of the structures due to these inertial loads causes vibration and cannot be disregarded. Many studies about aeroelasticity have been devoted to instability phenomena such as divergence, flutter, and control reversal. In these studies, the state equations have been linearized, and the stability analysis has been performed around the equilibrium point or the trim flight level.

One of the initial researchers (Kirsch, 1965) derived the equations of motion for a flexible projectile using

Lagrange's equations. This way, linearized equations of motion are transferred to the steady-state space to examine the projectile's stability. Mierovitch and Nelson (Mierovitch, 1966) used the same equations to study the aeroelastic stability of a high-spin satellite with flexible components. (Platus, 1992) investigated the stability and designed a controller for a spinning flexible projectile with a slender body. In this article, the associated equations of motion have been linearized around a trim-point condition then critical dynamic pressure and the roll spin velocity related to aeroelastic instability were determined.

Most of the studies about flexible projectile stability (Khoshnood, et al., 2010) & (Elyada, March-April 1989), are based on linearized equations of motion and transformed equations to state space. This study investigated the effects of the structure's stiffness distribution on the aeroelastic stability of the projectile and the optimum configuration with the highest values of dynamic pressure without divergence. As a result, the role of nonlinear and coupling expressions has been neglected. Of course, this linearization does not cause a significant inaccuracy in aeroelastic analysis, because if a linearized equation becomes unstable, an allowable range for the dynamic pressure would be more limited, resulting in a more conservative design, and also the stability margin is decreased (Shamaghdari & Nikravesh, 2012) & (Kantor & E. Raveh, 2019).

(Bernhammer, et al., 2017) & (Riso & Cesnik, 2023) introduce a new approach for aeroelastic analysis of slender flight vehicles with large deformation. They use the corotational method with a divided or meshed body method, in which the deformation of each segment is computed using a linear model in a local and then moved into its global position by applying large, rigid-body displacements.

In simulation-based or time-based stability analyses (Looye, 1999), there is no need for linearization and omitting coupling terms, so the equations can be applied in their original form (Chen, et al., August 2008) & (Silva, 2018); So, it is expected that better accuracy and perception for flight and stability behavior can be achieved (Pourtakdust & Assadian, 2004); This device can also predict field & experimental tests and reduce cost and time. However, for complex and complete geometries, experimental tests are at least necessary for verification (Ning, et al., 2016).

In time-based analyses, determination of the exact flight condition of instability, i.e., specified velocity and dynamic pressure, is difficult due to the continuous and gradual nature of the behavior of quantities (See Result section, item 9.4). In studies with time-domain analysis, (Gil Annes da Silva, et al., 2013) & (Sahu, 2006) have investigated the aeroelastic stability of a sounding rocket by using the Z-Aero software for simultaneous solving of the structural and aerodynamic equations. In this study, flutter analysis was performed based on the time variable generalized function.

The advantages of the flexible projectile simulation are not limited to stability analysis, which can be used in various areas such as guidance and control systems (M. da Fonseca, et al., 2007), (Khoshnood, et al., 2010) & (Khoshnood, et al., 2008), positioning and performance of sensor devices (Pourtakdust & Assadian, 2004), preliminary design (Kantor & E. Raveh, 2019), differences in aerodynamic loads, effects of follower force, i.e., stability problem due to thrust (wu, et al., 2012), (Xu, et al., 2016), (Chae, July 2004) and (Hodges, 2004), simulation and trajectory analysis, etc.

Simulation and trajectory analysis (collision accuracy) are investigated in this research. In practice, flight simulation is useful in preliminary design (Elyada, 1989) and optimization (Nikbay, et al., 2013). In the presented article we will show that in unguided projectiles (in the absence of control commands that cause lateral loads) with medium to high natural frequencies (conventional design with ordinary slenderness ratio and stiffness), the aeroelastic effects rarely lead to flight instability and only cause trajectory unmatching; Therefore, flexibility only changes the flight quantities and accuracies rather than changing the stability attitude. It will show that high inherent inaccuracies in thrust force increase lateral loads and therefore affect aeroelasticity, which can lead to instability other than mis-trajectories.

2. Extraction equations of motion

The velocity vector of each mass element ($\vec{V_i}$) which is used for computing kinetic energy, and wind-body angle distribution is computed by using the Coriolis law as follows (Elyada, 1989), (Kirsch, 1965), (Silva & Roberto, 2013), (Pourtakdust & Assadian, 2004) and (Platus, 1992):

$$\vec{V_i} = \begin{cases} U + Qz - Ry \\ V + Rx - Pz \\ W + Py - Qz \end{cases}_R + \begin{cases} Q\sum_{i=1}^{N_e}\phi_i\xi_i - R\sum_{i=1}^{N_e}\phi_i\eta_i \\ \sum_{i=1}^{N_e}\phi_i\eta_i - P\sum_{i=1}^{N_e}\phi_i\xi_i \end{cases}_E \tag{2.1}$$

$\eta_i(t)$ and $\xi_i(t)$ are the generalized coordinates or displacements in y and z directions of the body axis, respectively. In this paper, we intend to compare the contributions of rigid and elastic terms; thus, the equations have been designated by R and E subscripts, respectively. $\phi_i(x)$ is the mode shape function, which, according to the high slenderness ratio of most projectiles, is computed from the Euler-Bernoulli beam theory, subjected to axial force distribution $F_{axial}(x)$ with free-free conditions on its two ends; Structure deformations must also be in the linear ranges: So, $\phi_i(x)$ is taken from the following equation (Heng & Yin, September 2019) & (Xu, et al., 2016):

https://doi.org/cna.2025.hpsm-8n90

$$m(x)\omega_i^2\phi_i(x) + \frac{\partial^2}{\partial x^2}\left[E(x)I_{zz}(x)\frac{\partial^2\phi_i(x)}{\partial x^2}\right]x + \frac{\partial}{\partial x}\left[F_{axial}(x)\frac{\partial\phi_i(x)}{\partial x}\right] = 0 \tag{2.2}$$

$F_{axial}(x)$ is the distribution of axial force in the longitudinal axis of the projectile, which is computed as below (Xu, et al., 2016):

$$F_{axial}(x) = F_{thrust} - F_{axial\,drag}(x) - m(x) \times a_{axial} \tag{2.3}$$

In the above equation, $F_{Axial\,Drag}(x)$, is the axial aerodynamic drag force and a_{Axial} is the projectile's axial acceleration. Due to the infinite degrees of freedom in the motion of a flexible projectile, the Lagrangian approach was applied to derive the equations of motion. The equations (4-6) are related to translational motion; The equations (7-9) are related to rotational motion; Two groups of equations for transverse vibration (10 and 11) have the number as the considered modes (N_e) which are the generalized coordinates η_i and ξ_i are extracted from them respectively (Khoshnood, et al., 2010), (Khoshnood, et al., 2008) and (Raptis, 2007):

$$\dot{U} = \frac{F_x}{M} + \left[RV - QW - \dot{M}U\right]_R \tag{2.4}$$

$$\dot{V} = \frac{F_y}{M} + \left[PW - RU - \dot{M}V\right]_R \tag{2.5}$$

$$\dot{W} = \frac{F_z}{M} + \left[QU - PV - \dot{M}W\right]_R \tag{2.6}$$

$$\begin{aligned}\dot{P} = \frac{1}{I_{xx} + \sum_{i=1}^{N_c} m_i(\eta_i^2 + \xi_i^2)}\Big[M_x - i_{xx}P \\ + \Big(\sum_{i=1}^{N_c} m_i(\dot{\eta}_i\xi_i - \eta_i\dot{\xi}_i) \\ + (Q^2 - R^2)\sum_{i=1}^{N_c} m_i\eta_i\xi_i \\ - 2P\sum_{i=1}^{N_c} m_i(\dot{\eta}_i\dot{\xi}_i + \xi_i\dot{\xi}_i) \\ + QR\sum_{i=1}^{N_c} m_i(\xi_i^2 - \eta_i^2)\Big)\Big]\end{aligned} \tag{2.7}$$

$$\begin{aligned}\dot{Q} = \frac{1}{I + \sum_{i=1}^{N_c} m_i\xi_i^2}\Big[M_y - iQ + PR(I - I_{xx}) \\ + \Big(-PR\sum_{i=1}^{N_c} m_i\xi_i^2 \\ + (\dot{R} - PQ)\sum_{i=1}^{N_c} m_i\eta_i\xi_i \\ - 2Q\sum_{i=1}^{N_c} m_i\xi_i\dot{\xi}_i \\ + 2R\sum_{i=1}^{N_c} m_i\dot{\eta}_i\xi_i\Big)\Big]\end{aligned} \tag{2.8}$$

$$\begin{aligned}\dot{R} = \frac{1}{I + \sum_{i=1}^{N_c} m_i\eta_i^2}\Big[M_z - iR - PQ(I - I_{xx}) \\ + \Big(PQ\sum_{i=1}^{N_c} m_i\eta_i^2 \\ + (\dot{Q} + PR)\sum_{i=1}^{N_c} m_i\eta_i\xi_i \\ - 2R\sum_{i=1}^{N_c} m_i\eta_i\dot{\xi}_i \\ + 2Q\sum_{i=1}^{N_c} m_i\eta_i\dot{\xi}_i\Big)\Big]\end{aligned} \tag{2.9}$$

$$\begin{aligned}\dot{\eta}_i = \frac{Q\eta_i}{m_i} - 2\mu_i\omega_i\dot{\eta}_i + (P^2 + R^2 - \omega_i^2)\eta_i \\ + 2P\dot{\xi}_i + (\dot{P} - QR)\xi_i\end{aligned} \tag{2.10}$$

$$\begin{aligned}\dot{\xi}_i = \frac{Q\xi_i}{m_i} - 2\mu_i\omega_i\dot{\xi}_i + (P^2 + Q^2 - \omega_i^2)\xi_i \\ - 2P\dot{\eta}_i - (\dot{P} + QR)\eta_i\end{aligned} \tag{2.11}$$

In the above equations, M' indicates the ratio of the projectile's propellant burning rate or mass rate ($\dot{M}$) to the initial mass (M); The rate of the axial moment inertia (I_{xx}) can be ignored commonly due to its near-zero. In the equations of the translational velocities, the direct role of flexibility isn't seen due to a few simplistic assumptions. However, in equations related to angular velocities (equations 7-9), the direct role of flexibility is evident and non-negligible. It can also be observed that flexibility produces such new expressions or quantities that could not be pointed out in rigid equations. For example, the terms $\sum_{i=1}^{N_e} m_i\xi_i^2$ and $\sum_{i=1}^{N_e} m_i\eta_i^2$ are considered as elastic rotational inertia. These expressions also introduce coupling between the rigid and elastic expressions, which is ignored in stability analysis methods based on linearization.

https://doi.org/cna.2025.hpsm-8n90

3. Distribution of the wind-body angles

Unlike the rigid model, the angles of attack and sideslip of the flexible projectile (a_e, β_e) will be variable along the body due to its deformations and vibrations, so the distribution of the wind-body angles must be determined. According to the definition of these angles, their distribution can be expressed as:

$$\begin{aligned} a_e(x,t) = & \left[a_r - \frac{Qx_l(x)}{V_{co}} \right]_R \\ & + \frac{1}{V_{co}} \left[\sum_{i=1}^{N_e} \phi_i(x)\dot{\xi}_i(t) \right. \\ & + \frac{P}{V_{co}} \sum_{i=1}^{N_e} \phi_i(x)\eta_i(t) \\ & \left. - \sum_{i=1}^{N_e} \dot{\phi}_i(x)\xi_i(t) \right]_E \end{aligned} \tag{3.1}$$

$$\begin{aligned} \beta_e(x,t) = & \left[\beta_r + \frac{Rx_l(x)}{V_{co}} \right]_R \\ & + \frac{1}{V_{co}} \left[\sum_{i=1}^{N_e} \phi_i(x)\dot{\eta}_i(t) \right. \\ & - \frac{P}{V_{co}} \sum_{i=1}^{N_e} \phi_i(x)\dot{\xi}_i(t) \\ & \left. - \sum_{i=1}^{N_e} \dot{\phi}_i(x)\eta_i(t) \right]_E \end{aligned} \tag{3.2}$$

where $\left[a_r - \frac{Qx_l}{V_{co}} \right]_R$ and $\left[\beta_r + \frac{Rx_l}{V_{co}} \right]_R$ are the rigid parts of the wind body angles and the expressions related to flexibility are denoted by the subscript E. It should be noted that terms (a_r, β_r) just because of the similarity of the calculations shown by the subscript r and they indeed indirectly depended on the structure's deformation.

4. Calculation of the aerodynamic loads

The quasi-stable method is applied to calculate the aerodynamic loads so that the aerodynamic coefficients are multiplied by the instantaneous values of the wind-body angles (Yin, et al., 2016). This assumption is only valid for the cases where the structure's natural frequencies are remarkably higher than the aerodynamic loads changing frequencies (Gil Annes da Silva, et al., 2013) & (Elyada, 1989). Since the body coordinate has been used to describe the equations of motion, the aerodynamic coefficients and loads are expressed in the same coordinate instead of the stability coordinate. The general relation for calculating the aerodynamic loads is as follows (Looye, 1999):

$$F_{Ax'} F_{Ay'} F_{Az} = Q_{co} S_{ref} (C_x, C_y, C_z) \tag{4.1}$$

$$M_{Ax'} M_{Ay'} M_{Az} = Q_{co} S_{ref} d (C_i, C_m, C_n) \tag{4.2}$$

The subscript A represents the aerodynamic forces and moments. Due to the variation of the wind-body angles along the body, a distribution of aerodynamic coefficients should be used instead of constant values. In Figure 1, the distribution of the normal lift slope coefficients along the body length, i.e., C_y & C_z are shown in the different angles of attack (Hodges, 2004).

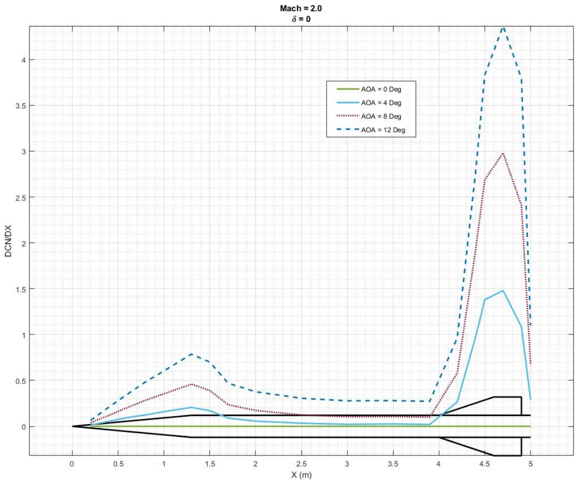

Figure 1. The case study geometry with its distribution of the normal force slope $C_{z\alpha}$ or $C_{y\beta}$

In general, the relations for calculating aerodynamic force (C_x, C_y, C_z) and moment (C_l, C_m, C_n) coefficients are (Shamaghdari & Nikravesh, 2012):

$$\begin{aligned} C_x = & \int_0^l \left(C_{x\alpha}(x)\alpha(x) + C_{x\beta}(x)\beta(x) \right) dx \\ & + C_{x0} + C_{xp} p \frac{d}{2V} + C_{x\delta}\delta \end{aligned} \tag{4.3}$$

$$\begin{aligned} C_y = & \int_0^l \left(C_{y\alpha}(x)\alpha(x) + C_{y\beta}(x)\beta(x) \right) dx \\ & + C_{y0} + C_{yp} r \frac{d}{2V} + C_{y\delta}\delta_r \end{aligned} \tag{4.4}$$

$$\begin{aligned} C_z = & \int_0^l \left(C_{z\alpha}(x)\alpha(x) + C_{z\beta}(x)\beta(x) \right) dx \\ & + C_{z0} + C_{zp} q \frac{d}{2V} + C_{z\delta}\delta_e \end{aligned} \tag{4.5}$$

$$\begin{aligned} C_l = & \int_0^l \left(C_{l\alpha}(x)\alpha(x) + C_{l\beta}(x)\beta(x) \right) dx \\ & + C_{l0} + C_{lp} p \frac{d}{2V} + C_{l\delta}\delta_a \end{aligned} \tag{4.6}$$

$$\begin{aligned} C_m = & \int_0^l \left(C_{m\alpha}(x)\alpha(x) + C_{m\beta}(x)\beta(x) \right) dx \\ & + C_{m0} + C_{mq} q \frac{d}{2V} + C_{m\delta}\delta_e \end{aligned} \tag{4.7}$$

https://doi.org/cna.2025.hpsm-8n90

$$C_n = \int_0^l \left(C_{n\beta}(x)\beta(x) + C_{n\delta}(x)\delta(x)\right) dx + C_{n0} + C_{np} r \frac{d}{2V} + C_{n\delta}\delta_r \tag{4.8}$$

Due to the geometry and flight conditions, not all of the aerodynamic coefficients have the same effect and importance; For example, some derivatives such as $C_{Z\alpha}$ and $C_{Y\beta}$ can be negligible compared to the $C_{Z\alpha}$ and $C_{Y\beta}$ coefficients. Even though it is necessary to pay attention to the wind-body angle rates compared to their magnitudes. Also, it is important to consider the effects of the angular velocities in the wind-body angular distribution, i.e.,

$$\frac{Qx_1(x)}{V_\infty} \quad \text{and} \quad \frac{Rx_1}{V_\infty}$$

are considered, then the aerodynamic coefficients C_{Zq}, C_{Yr}, C_{nr} and C_{mq} should be eliminated in aerodynamic load calculations. There is another way to keep them and remove terms

$$\frac{Qx_1}{V_\infty} \quad \text{and} \quad \frac{Rx_1}{V_\infty}$$

from the wind-body angle distribution: In this way, aerodynamic coefficients can be computed as below:

$$C_{l\alpha} = \int_0^l C_{x\alpha}(x) x_l(x) dx \quad \& \quad C_{l\beta} = \int_0^l C_{x\beta}(x) x_l(x) dx \tag{4.9}$$

$$C_{m\alpha} = \int_0^l C_{z\alpha}(x) x_l(x) dx \quad \& \quad C_{m\beta} = \int_0^l C_{z\beta}(x) x_l(x) dx \quad \& \quad C_{z\alpha} = \frac{2}{d}\int_0^l C_{z\alpha}(x) x_l(x) dx \tag{4.10}$$

$$C_{n\beta} = \int_0^l C_{y\beta}(x) x_l(x) dx \quad \& \quad C_{n\gamma} = \int_0^l C_{y\gamma}(x) x_l(x) dx \quad \& \quad C_{y\gamma} = \frac{2}{d}\int_0^l C_{y\beta}(x) x_l(x) dx \tag{4.11}$$

The aerodynamic coefficients can be calculated using any numerical or reliable analytical method. The coefficients that are considered without distribution along the body like $C_{l0}, C_{m0}, C_{n0}, C_{zq}, C_{xq}, C_{lr}, C_{lp}, C_{yp}$ etc are called rigid aerodynamic coefficients. These coefficients are independent of the distribution of wind-body angles and can be called from previous lookup tables of the rigid one. As mentioned, the other derivatives such as $C_{n\beta}$ and $C_{m\alpha}$ are also calculated indirectly by taking moments from the aerodynamic force coefficients distribution relative to the C.G. according to equations (23) to (24).

5. Thrust force inclination due to body deformations

Thrust deviation initially produced by inherent deviation from manufacturing inaccuracy and structure deformation in flight: These undesirable forces and moments cause mal-trajectory, miss-targeting, flight instability, and unwanted effects on the guidance loop. The inherent error can be modeled as fixed or random values (for example, white noise with the Gaussian model), either of which can be true depending on the conditions of the problem. In this study, constant values are considered for this. Structural deformations are almost caused by lateral loads, which in turn depend on aerodynamic factors, command loads, and the inherent deviation of the propulsion. The components of the thrust force due to the inherent deviation and structure deformation ($F_{T_{Deviation}}$) are calculated as below (Xu, et al., 2016):

$$F_{T_{Deviation}} = \begin{Bmatrix} \cos\theta_{Tx-y}\cos\theta_{Tx-z} \\ \sin\theta_{Tx-y}\cos\theta_{Tx-z} \\ -\sin\theta_{Tx-z} \end{Bmatrix} F_{T_{Thrust}} \tag{5.1}$$

Which θ_{Tx-y} and θ_{Tx-z} are the total (inherent deviation + structural deformation) deviation angles of the thrust force related to the xy and xz planes and computed as below:

$$\theta_T = \theta_r + \theta_x$$

$$\begin{cases} \theta_{T_{x-y}} = \theta_{I_{x-y}} + \theta_\eta \\ \theta_{T_{x-z}} = \theta_{I_{x-z}} + \theta_\xi \end{cases} \tag{5.2}$$

θ_{Ix-y} and θ_{Ix-z} are the inherent deviation angles of the thrust force related to the xy and xz planes; The elastic deflection angles ($\theta_{\eta_e}, \theta_{\xi_e}$) are also calculated as follows (Khoshnood, et al., 2008):

$$\theta_{\eta_e}(t) = \sum_{i=1}^{\infty} \phi_i(x_{thrust})\eta_i(t) \qquad \theta_{\xi_e}(t) = \sum_{i=1}^{\infty} \phi_i(x_{threshold})\xi_i(t) \tag{5.3}$$

By substituting relation (27) into (26) and then into (25), the components of the deviated thrust force vector are obtained as follows:

$$\vec{F}_{T_{Deviation}} = \begin{Bmatrix} \cos\left(\theta_{Ix-y} + \sum_{i=1}^{\infty}\phi_i(x_{thrust})\eta_i(t)\right) \cos\left(\theta_{Ix-z} + \sum_{i=1}^{\infty}\phi_i(x_{threshold})\xi_i(t)\right) \\ \sin\left(\theta_{Ix-y} + \sum_{i=1}^{\infty}\phi_i(x_{thrust})\eta_i(t)\right) \cos\left(\theta_{Ix-z} + \sum_{i=1}^{\infty}\phi_i(x_{threshold})\xi_i(t)\right) \\ -\sin\left(\theta_{Ix-z} + \sum_{i=1}^{\infty}\phi_i(x_{thrust})\xi_i(t)\right) \end{Bmatrix} T \tag{5.4}$$

Which $\dot{\phi}_i(x_{thrust})$ is the derivation (slope) of the eigenfunctions at the acting point of the thrust force; Finally, the thrust moment caused by the elastic and inherent deflection ($M_{T_{Deviation}}$) is calculated from the equation below:

$$M_{T_{Deviation}} = F_{T_{Deviation}} \times r_{T_{Deviation}} \tag{5.5}$$

The distance of the thrust force's acting point relative to the instantaneous projectile's C.G. position, namely $r_{T_{Deviation}}$ is calculated by the way of equation (30):

$$\vec{r}_{T_{Deviation}} = \begin{pmatrix} \Delta_{T_{x-y}} + \sum_{i=1}^{\infty} \phi_i(x_{thrust})\eta_i \\ \Delta_{T_{x-z}} + \sum_{i=1}^{\infty} \phi_i(x_{thrust}) z_i \end{pmatrix} \tag{5.6}$$

Which $\Delta_{T_{x-y}}$ and $\Delta_{T_{x-z}}$ are the inherent eccentricity of the thrust force in xy and xz planes; The thrust function or curve is another important item in flight stability and aeroelastic response; Various thrust functions, even with the same propulsion energy, have different effects on the mentioned items; Because various thrust functions have different propulsion-specific impulses (I_{sp}), burning times, and mass rate; So, they have different rates of mass and moment of inertia ($\dot{m}$ & $\dot{I}$), different natural frequency variations. All of these properties are important factors in aeroelastic response and flight stability. According to (Equations 4 & 5), various thrust functions result in different mass rates and consequently different variations in axial force and natural frequencies; These items are very influential in aeroelastic behavior (See result section).

6. Case Study and input data

In this article, a case study is a flexible projectile with propulsion; The projectile's geometry is shown in Figure 1. In most articles related to stability analysis of flexible projectiles, case studies are with no thrust force, and especially with any inaccuracy in it (Elyada, 1989). These inherent inaccuracies, comprised of structural deformation, produce unwanted and unpredictable force and moment elements that cause miss-distance, undesirable trajectory, flight instability, and other adverse consequences. All of the input data and properties that are used for simulation are presented in Table 2, and the nomenclature is given in Table 1.

7. Modeling & simulating

All of the equations and relations of the flexible projectile's motion are modeled in the Simulink environment of MATLAB software (J. Diston, 2009), (Gupta, 1991) & (Khoshnood, et al., 2008); This environment provides users marvelous capabilities such as lookup tables, math functions, display & monitoring tools, block-diagram & module-form structure, etc. Simulation's subsystems include N-DOF equations of motion, Environment conditions, Wind-body angles distribution, Aerodynamic loads, Thrust & Mass functions, Generalized Forces, Stability checking, Dynamic stresses and strains, etc. Figure 2 shows a section of this simulation; Some blocks may themselves contain many sub-block diagrams, look-up tables, interface codes, etc.

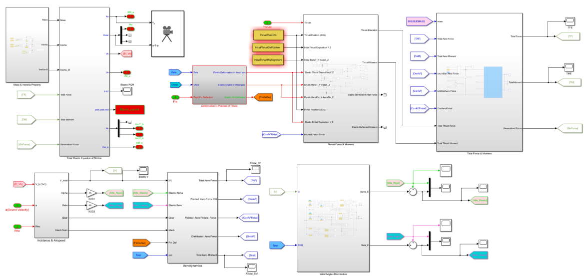

Figure 2. A section from the home page of flexible projectile flight simulation software.

The Blocks Equations of motion and orientation, Calculation of aerodynamic loads, Effects of propulsion's deflection, Generalized loads, and Resultant of forces and moments are known.

8. Making the simulation faster

A great novelty in this research is the implementation of look-up tables made from some pre-computed calculations to reduce run-time computations and increase simulation velocity. As mentioned before, for computing aerodynamic loads (Equations 14 & 15), the distribution of the aerodynamic coefficients as well as $\alpha(x)$ and $\beta(x)$, must be determined according to the structure deformations for various flight conditions at each time step. These are time-consuming processes and impair the real-time capability of the simulation. To alleviate the problem, the distribution of aerodynamic coefficients and their multiplication expressions were pre-calculated and imported as look-up tables. During simulation, the required data is just called from look-up tables depending on the segment under consideration on the body, mode number, and flight conditions. The same procedure is also used for the aerodynamic and generalized loads computations. This strategy remarkably enhances the simulation run speed while retaining the advantages of a real-time and elastic simulation and can be used in onboard flight computers. The methodology has been implemented in the Simulink environment of MATLAB software, as shown in Figure 3 in which the lookup tables are distinguishable by the yellow color blocks.

During simulation, the required data are just called from look-up tables according to the geometry's element number, mode number, and aerodynamic conditions, including wind-body angles values, Mach, and Reynolds numbers. We use this process to compute the aerodynamic & generalized loads and wind-body angle distributions. Using this strategy, the simulation run speed is significantly increased, and it can perform real-time simulations used in onboard flight processors or computers.

https://doi.org/cna.2025.hpsm-8n90

Table 1. Nomenclature: Latin and Greek characters

Latin Characters		Latin Characters	
d	Projectile diameter (m)	Q_∞	Aerodynamic pressure (Pa)
F_x, F_y, F_z	Resultant forces in body coordinate	S_{ref}	Aerodynamic reference surface (m^6)
F_{thrust}	Projectile's thrust force	V_∞	Speed of free stream (m/s)
$I_{yy} = I, I_{xx}$	Moment of inertia $(kg \cdot m^2)$	$x_l(x)$	Distance from C.G. to mesh for aerodynamics
l	Projectile's length	x_{thrust}	Distance of thrust from C.G.
M_x, M_y, M_z	Resultant moments in body coordinate	$[x\ y\ z]$	Vector components from C.G. to mass element
m_i	Generalized mass for vibration modes	U, V, W	Linear velocity components of C.G.
$m(x)$	Mass distribution of projectile	P, Q, R	Angular velocity components
Q_{q_i}	Generalized loads for q_i (η_i & ξ_i)		
Greek Characters		**Greek Characters**	
μ_i	Generalized damping coefficient	$\rho(x)$	Density distribution along body
ω_i	Natural frequencies of projectile	ϕ, θ, ψ	Euler angles (rad)

Table 2. Input data for simulation

Parameter		Value	
Initial mass (Full fuel)	1800 kg	Final mass (Empty fuel)	1000 kg
Projectile length	5 m	Projectile diameter	0.5 m
Booster length	2.54 m	Booster diameter	0.7 m
Thrust magnitude	(80, 130, 400) kN	Thrust burning time	(30 & 15) s
Initial thrust misalignment	1 mm for xy & xz planes	Initial thrust deviation	$0.1°$ about xy & xz planes
Initial velocity (U_0, V_0, W_0)	$(10, 0, 0)$ m/s	Initial angular velocity (P_0, Q_0, R_0)	$(0, 0, 0)$ rad/s
Initial position	$(0, 0, 10)$ m	Initial Euler angles $(\psi_0, \theta_0, \phi_0)$	$(0, 50, 0)°$
Natural frequencies (Hz)			
High stiffness		Medium stiffness	
36, 100, 197, 326, 488, 681, 907		18, 51, 164, 245, 343, 456	
Generalized damping ratio			
0.01, 0.02, 0.03, 0.05, 0.07, 0.11, 0.15			

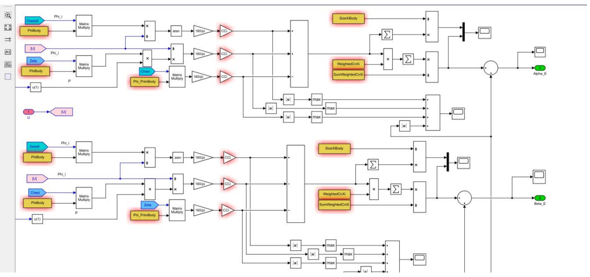

Figure 3. A section from the block diagram related to calculating the wind-body angle distribution. Look-up tables are seen as yellow rectangular blocks.

9. The simulation validation and reliability

Validation of the input quantities includes the aerodynamic coefficient distribution, mass distribution, stiffness, natural frequencies, and vibration modes. For the aerodynamic coefficients, the resultant of the distribution of the elastic coefficients and their resultant moment about the C.G. (for the moment coefficients) must be equal to the rigid coefficients. According to Figure 1, to validate the distribution of the aerodynamic coefficients, their integral, and also their moment about the C.G., according to each α or β must be equal to the amount of the normal force coefficients $C_{N\alpha}$ (which is $C_{z\alpha}$ or $C_{y\beta}$) and the corresponding aerodynamic moment coefficients, i.e., $C_{m\alpha}$ or $C_{n\beta}$ in the rigid model (Yuan, et al., 2021). For the simulation verification and validation, approaches are extensive and somewhat complicated, and the discussion about this is out of the scope of this article. But briefly, it can be said that some standard maneuvers and flight conditions are used in this about. In the presented article, we have a rigid body simulation that was validated with so many cases and field tests. As expected, when structure stiffness tends to have high values, both the rigid and elastic models must show the same behavior and results, which will be shown in the following (Result-Section 10.1).

10. Results & Discussions

It is predicted that from the equations of motion and other constitutive relations that some design parameters like structure stiffness which is often represented by natural frequencies, thrust force function and its misalignment or inaccuracies, rolling velocity, rate of mass, and moment of inertia variation, initial and boundary conditions, aerodynamic condition, command loads, etc., have remarkable impacts on a flexible projectile trajectory and instability. The role of structure stiffness, thrust force function, and its inaccuracies have been studied in this research and are discussed in this section. Other parameters will be discussed in our future research.

10.1 Effects of the structure flexibility (natural frequency) on thrust deviation

Stiffness is defined as resistance to deformation, so a projectile with a stiff structure (in high natural frequencies) has limited deformations, and it is expected that

https://doi.org/cna.2025.hpsm-8n90

the flight behavior of an elastic projectile is similar to a rigid one. As mentioned before, this can be used for simulation validation. From Figure 4, it can be seen that two rigid and elastic simulations match each other and there is no difference in trajectory (Figure 4a) and thrust force components (Figure 4b).

In rigid simulation, the resulting lateral forces and moments would be zero if the thrust vector had no inherent inaccuracy. However, they may exist in elastic simulations due to the structural deformations. Inherent inaccuracy in structure, often from defects and errors in production, is the most common reason for unmatching the rigid and the elastic simulation (real test). In low stiffness or flexible structures with low natural frequencies, deformations and accordingly differences between two simulations become greater and more observable (Figure 5a). In the thrust flexible projectile, structure deformation causes thrust deviation whose undesired force and moment components lead to miss-trajectory and instability (Figure 5b). It will be shown that this issue is also affected by inherent inaccuracies and thrust function (See Figures 6a & 6b). From Figures 5a & 5b, it can be concluded that under non-critical loading and a high degree of rigidity of the projectile's structure, we expect small differences between the rigid and flexible simulations. However, differences in the flight path and other flight parameters are very slight due to the absence of moments arising from structural deformations.

10.2 Effects of the thrust force function

Often it is not easy to assess the difference in flight trajectory and the miss-distances, because the structure's natural frequency increases with the decrease in the propellant burning time, while the induced lateral loads and acceleration increase (wu, et al., 2012). We are eager to investigate the effect of the thrust function by keeping its resultant energy. In this regard, we halved the thrust's burning time, so the thrust force doubled. From Figure 6a, it can be seen that axial acceleration and differences between the two simulations increased by decreasing in thrust burning time. The shorter thrust burning time resulted in greater values of $\dot{m}$ & $\dot{I}$, which led to changes in natural frequencies (Khoshnood et al., 2008), thereby causing greater differences between the two simulations exactly at the moment the thrust force is turned off/on. However, due to the reduced burning time, the differences in flight trajectory are reduced at the same flight time (See Figure 6b); Hence due to the changing in thrust specific impulse, reducing in burning time leads to the greater. It can be seen that by reducing burning time and increasing thrust force magnitude.

As expected, in the presence of thrust deviation, remarkable differences can be pointed out between the rigid and flexible simulations. Figure 6a also shows a jump in lateral accelerations when the propulsion is turned on/off. By the way, the induced lateral accelerations and vibrations are damped due to the structural damping, and as a consequence, the two simulations give nearly the same results.

10.3 Effects of the Thrust Inaccuracies

In the presence of thrust deviation, we expect that differences between two rigid and elastic simulations become more obvious. Another propulsion-related issue is inaccuracies in exit thrust, which affects flight trajectory and stability. Here, according to the nature of the inaccuracies, two kinds of inherent errors are defined: out-centering and deviation angle. In this stage of the study, we used these values: 0.1 mm for out-centering and 0.1° for deviation about xy and xz planes. These inherent inaccuracies increase lateral forces and induced moments, which increase the effect of aeroelasticity and therefore increase structure deformation and trajectory mismatching. From Figure 7a it can be seen that differences in the two simulations increase especially when the thrust force is turned on/off. Hence, in this condition, more lateral acceleration and loads are exerted on the flexible projectile, which can lead to trajectory mismatching and flight instability. It can be observed from Figure 7b compared with Figure 6b that differences in flight trajectory increase incrementally due to the thrust inaccuracies.

10.4 Flight instability

The flexible projectile is expected to become unstable due to the exerted components of the deviated thrust when its structural stiffness or thrust's inherent inaccuracies come to their critical values. To see this, we increase inherent thrust deviation to 0.2° for the projectile with medium structure stiffness. It can be concluded from Figure 8 that the projectile became unstable because the values of the generalized coordinates, namely the amplitude of the oscillations, increased radically. Instability is a time-dependent phenomenon that occurs over a short time (XueRui, et al., 2007); In other words, instability occurs when a quantity exceeds its allowed or logical value, for example, an extreme deformation or mechanical stresses greater than ultimate strength. It can be observed in Figure 9 a critical or illogical value for the structure deformation (Chae, July 2004).

11. Conclusions

The results of the elastic simulation have been compared to the rigid simulation in this paper. In a conventionally designed projectile with a slenderness ratio of less than 15, the aeroelasticity seldom causes flight instability. It can be said that it just changes the flight quantities and the range and accuracy of the projectile. In these cases, the important factors in projectile instability are the thrust function and its inherent inaccuracies, when the aeroelastic issue comes into play. It was shown that the differences between rigid and flexible simulations increase by increasing the flexibility of the structure and the initial inaccuracy in thrust force. Furthermore, the effect of body deformation on the inherent deflection of thrust as well as on the stability and flight trajectory of the flexible projectile was evaluated. It was shown that in a rigid simulation, it is impossible to study the effects of the structure's stiffness and its causing thrust vector

https://doi.org/cna.2025.hpsm-8n90

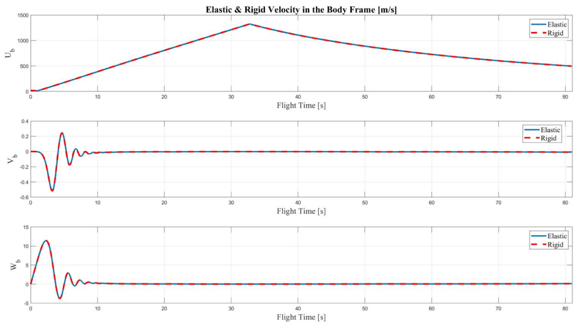

(a) Linear velocities in body axes

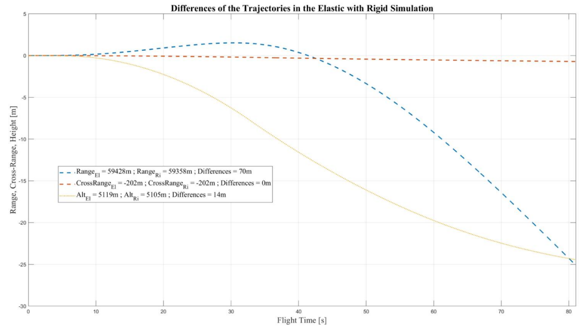

(b) Differences in trajectory components

Figure 4. The linear velocities in body axes (a) and differences in trajectory components (b) in two rigid and elastic simulations, in the case of a high stiffness structure.

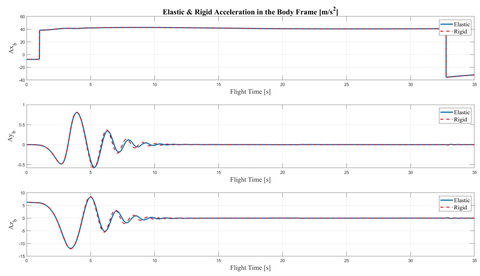

(a) Linear accelerations in body axes

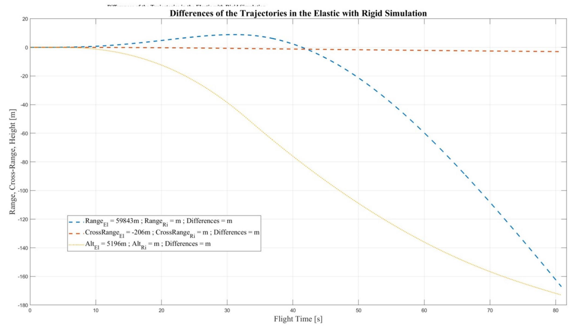

(b) Differences in trajectory components

Figure 5. The linear accelerations in body axes (a) and differences in trajectory components (b) in two rigid and elastic simulations; In the case of a medium stiffness structure and thrust burning time of 30 seconds.

deviation on flight stability. It can be said that when the projectile is simulated with no guidance commands, the main factor that causes the difference between the results of the two simulations is the deviations in the thrust vector due to flexibility, whose effects are more pronounced than the projectile's velocity and related dynamic pressure. It was also shown, instability is a time-dependent phenomenon that occurs over a short time; In other words, instability occurs when a quantity exceeds its allowed or logical value. By using simulation or time-domain stability analysis, it is too hard to determine a specific time for the onset of instability, but these provide a better perception of the projectile's flight behavior to the analyzer.

Authors contributions
All the authors have participated sufficiently in the intellectual content, conception and design of this work or the analysis and interpretation of the data (when applicable), as well as the writing of the manuscript.
Availability of data and materials
The data that support the findings of this study are available from the corresponding author upon reasonable request.
Conflict of interests
The authors declare that they have no known competing financial interests or personal relationships that could have appeared to influence the work reported in this paper.
Open access
This article is licensed under a Creative Commons Attribution 4.0 International License, which permits use, sharing, adaptation, distribution and reproduction in any medium or format, as long as you give appropriate credit to the original author(s) and the source, provide a link to the Creative Commons license, and indicate if changes were made. The images or other third party material in this article are included in the article's Creative Commons license, unless indicated otherwise in a credit line to the material. If material is not included in the article's Creative Commons license and your intended use is not permitted by statutory regulation or exceeds the permitted use, you will need to obtain permission directly from the OICC Press publisher. To view a copy of this license, visit https://creativecommons.org/licenses/by/4.0.

References

[1] L. O. Bernhammer, R. De Breuker, and M. Karpel. Geometrically nonlinear structural modal analysis using fictitious masses. *AIAA Journal*, 55(10): 3584–3593, 2017. DOI: https://doi.org/10.2514/1.J054787.

[2] S. Chae. *Effect of Follower Forces on Aeroelastic Stability of Flexible Structures*. PhD thesis, School of Aerospace Engineering, Georgia Institute of Technology, July 2004. In Partial Fulfillment of the Requirements for the Degree Doctor of Philosophy.

[3] P. Chen, D. H. Baldelli, and J. Zeng. Dynamic flight simulation (dfs) tool for nonlinear flight dynamic simulation including aeroelastic effects. In *AIAA Atmospheric Flight Mechanics*

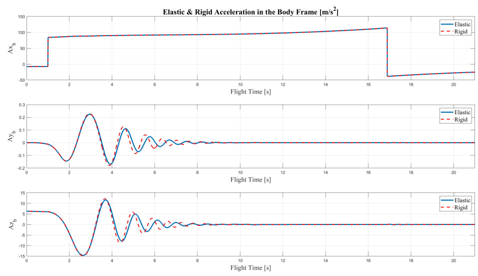

(a) Linear accelerations in body axes

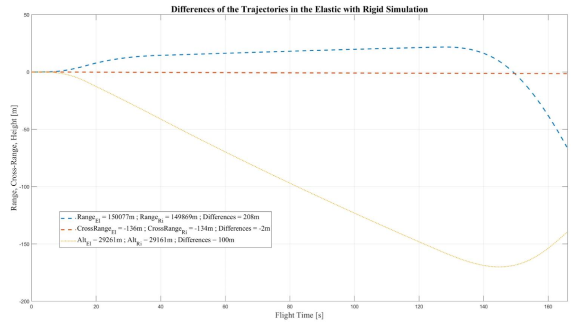

(b) Differences in trajectory components

Figure 6. The linear accelerations in body axes (a) and differences in trajectory components (b) for two rigid and elastic simulations; In the case of a medium stiffness structure and thrust burning time of 15 seconds.

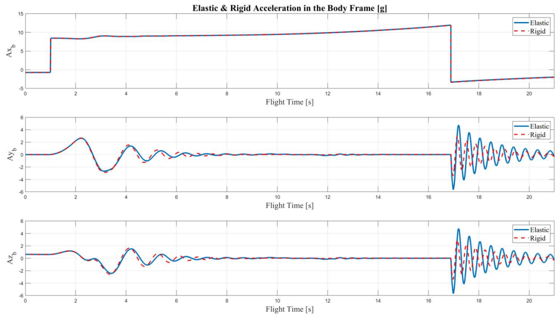

(a) Linear accelerations in body frame

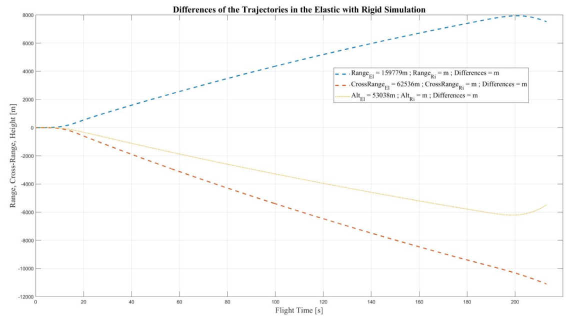

(b) Differences in trajectory components

Figure 7. The linear accelerations in body frame (a) and differences in trajectory components (b); In the case of a medium stiffness, a burning time of 15 sec, an inherent inaccuracy of thrust 0.1° for deviation, and 1 mm for misalignment.

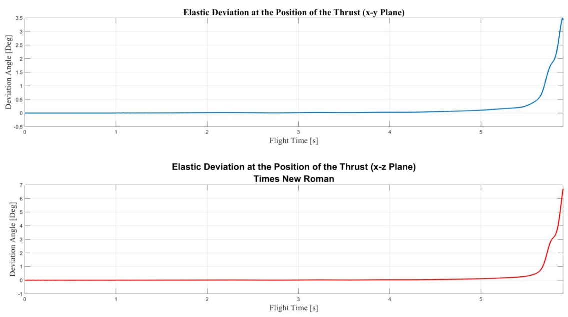

Figure 9. The deviation angles of the structure at the thrust position for the flexible projectile in elastic simulation; In the case of medium stiffness, inherent thrust deviation of 0.2° and a misalignment of 1 mm.

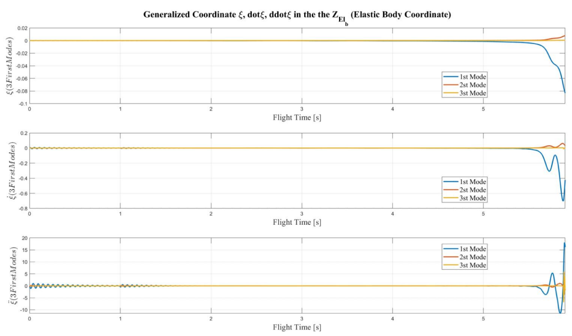

Figure 8. The generalized coordinates and their derivatives for the flexible projectile in elastic simulation; In the case of medium stiffness, inherent thrust deviation of 0.2° and a misalignment of 1 mm.

Conference and Exhibit, Honolulu, Hawaii, August 2008. DOI: https://doi.org/10.2514/6.2008-6376.

[4] D. Elyada. Closed-form approach to rocket-vehicles aeroelastic divergence. *Journal of Spacecraft and Rockets*, 26(2):95–102, March-April 1989. DOI: https://doi.org/10.2514/3.26038.

[5] D. Elyada. Closed-form approach to rocket-vehicles aeroelastic divergence. *Journal of Spacecraft and Rockets*, 26(2):95–102, March-April 1989. DOI: https://doi.org/10.2514/3.26038.

[6] R. Gil Annes da Silva, J. Guido Damilano, and J. L. F. Azevedo. A sensitivity investigation on the aeroelastic dynamic stability of slender spinning sounding rockets. *Journal of Aerospace Technology and Management*, 5(1):15–26, Jan-Mar 2013. DOI: https://doi.org/10.5028/jatm.v5i1.192.

[7] K. Gupta. An integrated general-purpose finite element structural, aeroelastic, and aeroservoelastic analysis computer program. Technical report, NASA, National Aeronautics and Space Administration, 1991.

[8] P. H. Zipfel. *Modeling and Simulation of Aerospace Vehicle Dynamics*. AIAA Education Series, 2001.

[9] L. Heng and Z. Yin. Effects of rotational motion on dynamic aeroelasticity of flexible spinning missile with large slenderness ratio. *Aerospace Science and Technology*, 94:105384, September 2019.
DOI: https://doi.org/10.1016/j.ast.2019.105384.

[10] D. H. Hodges. A new approach to aeroelastic response, stability and loads of missiles and projectiles. Technical report, U. S. Army Research Office, P.O. Box 12211, Research Triangle Park, NC 27709-2211, Atlanta, Georgia 30332-0150, 2004.

[11] D. J. Diston. *Computational Modelling and Simulation of Aircraft and the Environment*. John Wiley and Sons, Ltd., Publication, West Sussex, United Kingdom, 2009.
DOI: https://doi.org/10.1002/9781118536407.

[12] A. J. L. F. Transonic aeroelastic analysis of launch vehicle configuration. Technical Report CR-4186, NASA, 1998.

[13] E. Kantor and D. E. Raveh. Nonlinear structural, nonlinear aerodynamic model for static aeroelastic problems. *AIAA Journal*, 57(5):2158–2170, 2019.
DOI: https://doi.org/10.2514/1.J057309.

[14] A. Khoshnood, J. Roshanian, A. A. Jafari, and A. Khaki Sedigh. An adjustable model reference adaptive control for a flexible launch vehicle. *Journal of Dynamic Systems, Measurement, and Control*, 132(4):041010, 2010.
DOI: https://doi.org/10.1115/1.4001709.

[15] A. Khoshnood, J. Roshanian, and A. Khaki Sedig. Model reference adaptive control for a flexible launch vehicle. *Proceedings of the Institution of Mechanical Engineers, Part I: Journal of Systems and Control Engineering*, 222(1):49–55, February 2008.
DOI: https://doi.org/10.1243/09596518JSCE469.

[16] A. Kirsch. Dynamics equations of motion for flexible vehicles. Technical Report TIS-65SD310, General Electric Co., August 1965.

[17] G. Looye. Integrated flight mechanics and aeroelastic aircraft modeling using object-oriented modeling techniques. In *AIAA American Institute of Aeronautics and Astronautics*, volume 99, page 4192, 1999.

[18] T. Lu, X. Wu, J. Lei, and J. Yin. Numerical study on the aerodynamic coupling effects of spinning and coning motions for a finned vehicle. *Aerospace Science and Technology*, 77:399–408, 2018.
DOI: https://doi.org/10.1016/j.ast.2018.03.027.

[19] I. M. da Fonseca, M. B. P., and A. R. da Silva. Structural control interaction for an lss attitude control system using thrusters and reaction wheels. *Acta Astronautica*, 60(10-11):865–872, 2007.
DOI:
https://doi.org/10.1016/j.actaastro.2006.11.008.

[20] L. Mierovitch and H. Nelson. On the high-spin motion of a satellite containing elastic parts. *Journal of Spacecraft and Rockets*, 3(11): 1597–1602, 1966.
DOI: https://doi.org/10.2514/3.28713.

[21] M. Nikbay, N. Fakkusoglu, and M. Fakkusoglu. Reliability-based multidisciplinary optimization of aeroelastic systems with structural and aerodynamic uncertainties. In *13th AIAA/ISSMO Multidisciplinary Analysis Optimization Conference*, Fort Worth, Texas, September 2010.
DOI: https://doi.org/10.2514/6.2010-9187.

[22] Y. Ning, W. Nan, Z. Xin, and L. Wei. Nonlinear flutter wind tunnel test and numerical analysis of folding fins with freeplay nonlinearities. *Chinese Journal of Aeronautics*, 29(1):144–159, 2016.
DOI: https://doi.org/10.1016/j.cja.2015.12.011.

[23] D. Platus. Aeroelastic stability of slender, spinning missiles. *Journal of Guidance, Control and Dynamics*, 15(1):144–155, 1990.
DOI: https://doi.org/10.2514/3.20812.

[24] S. H. Pourtakdust and N. Assadian. Aeroelastic analysis of guided hypersonic launch vehicles. *Scientia Iranica*, 11(1):26–36, April 2004.

[25] C. Riso and C. E. Cesnik. Geometrically nonlinear effects in wing aeroelastic dynamics at large deflections. *Journal of Fluids and Structures*, 120:103897, 2023.
DOI:
https://doi.org/10.1016/j.jfluidstructs.2023.103897.

[26] J. Sahu. Time-accurate computations of free-flight aerodynamics of a spinning projectile with flow control. In *Conference Proceedings*, Colorado, USA, 2006.

[27] S. Shamaghdari and S. Nikravesh. A nonlinear stability analysis of elastic flight vehicle. *Aircraft Engineering and Aerospace Technology*, 84(6): 404–412, 2014.
DOI:
https://doi.org/10.1108/00022661211272954.

[28] S. Shamaghdari and S. Nikravesh. A nonlinear stability analysis of elastic flight vehicle. *Aircraft Engineering and Aerospace Technology: An international journal*, 84(6):404–412, 2012.
DOI:
https://doi.org/10.1108/00022661211272954.

[29] G. A. d. Silva and L. F. Roberto. A sensitivity investigation on the aeroelastic dynamic stability of slender spinning sounding rockets. *Journal of Aerospace Technology and Management*, 5(1): 12–26, 2013.
DOI: https://doi.org/10.5028/jatm.v5i1.192.

[30] W. A. Silva. Aerom: Nasa's unsteady aerodynamic and aeroelastic reduced-order modeling software. *Aerospace (MDPI)*, 5(2):41, 2018.
DOI: https://doi.org/10.3390/aerospace5020041.

[31] L. Wu, C. Xie, and C. Yang. Aeroelastic stability of a slender missile with constant thrust. In *Procedia Engineering*, volume 31, pages 128–135, Beijing, China, 2012.
DOI: https://doi.org/10.1016/j.proeng.2012.01.1002.

[32] M. XueRui, Y. ShuXing, and X. Yong. Coning motion stability of wrap around fin rockets. *Science in China Series E: Technological Sciences*, 50(1):1–9, 2007.
DOI: https://doi.org/10.1007/s11431-007-0026-0.

[33] T. Xu, J. Rong, D. Xiang, C. Pan, and X. Yin. Dynamic modeling and stability analysis of a flexible spinning missile under thrust. *International Journal of Mechanical Sciences*, 119:144–154, September 2016.
DOI: https://doi.org/10.1016/j.ijmecsci.2016.09.027.

[34] J. Yin, J. Lei, X. Wu, and T. Tianyu. Aerodynamic characteristics of a spinning projectile with elastic deformation. *Aerospace Science and Technology*, 51(1):181–191, 2016.
DOI: https://doi.org/10.1016/j.ast.2016.02.010.

[35] J. Yin, J. Lei, X. Xu, and T. Lu. Aerodynamic characteristics of a spinning projectile with elastic deformation. *Aerospace Science and Technology*, 51:181–191, 2016.
DOI: https://doi.org/10.1016/j.ast.2016.02.010.

[36] W. Yuan, S. Rimple, and D. Poire. Fully coupled aeroelastic analyses of wing flutter towards application to complex aircraft configurations. *Journal of Aerospace Engineering (ASCE)*, 34(2), 2021.
DOI: https://doi.org/10.1061/(ASCE)AS.1943-5525.0001232.

https://doi.org/cna.2025.hpsm-8n90